Visual Methods for Interpreting Optical Nonlinearity at the Molecular Level

RONALD D. WAMPLER,[†] ANDREW J. MOAD,[†] CHARLES W. MOAD,[‡] RANDY HEILAND,[‡] AND GARTH J. SIMPSON*[,†]

Department of Chemistry, Purdue University, West Lafayette, Indiana 47907, and Scientific Data Analysis Lab, Indiana University-Purdue University Indianapolis, Indianapolis, Indiana 46202

Received April 20, 2006

ABSTRACT

The emergence of nonlinear optical (NLO) measurement approaches has provided new windows into molecular and macromolecular structure within thin films and materials. The greatest barriers in mining this structural information increasingly appear in meaningfully relating these macroscopic results back to molecular-level descriptions, driven largely by the increasing complexity of the molecular systems and interfacial architectures under interrogation. As NLO methods continue their expansion into increasingly diverse disciplines, so grows the need for tools to guide this evolution without sacrificing the mathematical rigor of more traditional tensor representations. Recent developments reviewed in this Account are designed to facilitate interpretation of complex assemblies using relatively simple but still quantitatively accurate visual representations of the polarization-dependent optical nonlinearity, both for individual chromophores and for polymeric assemblies of coupled chromophores. Although the primary focus of this Account is on second-order nonlinear optical effects, including second harmonic generation and sum frequency generation, many of these same concepts also directly apply to higher-order phenomena.

Introduction

Remarkable and wonderful interactions between light and matter arise in intense optical fields. Practical applications of these nonlinear optical (NLO) processes were enabled with the advent of lasers. The first definitive observation of a NLO interaction was in 1961 by Franken and coworkers, in which second harmonic generation (SHG, Figure 1) was demonstrated in a quartz crystal using a millisecond pulsed ruby laser.[1] Since these early days, the field of nonlinear optics has grown rapidly, driven largely by the ever-increasing availability of short-pulsed lasers combined with the unique capabilities and information content of NLO measurements. The symmetry of even-ordered NLO processes such as SHG and sum frequency generation (SFG, Figure 1) have allowed for unprecedented surface selectivity using optical methods. In the case of SHG, relatively simple and inexpensive instruments routinely yield sub-monolayer surface sensitivity. Most importantly for the present purposes, the coherent nature of NLO effects allows access to exquisite molecular and macromolecular structural information from the polarization dependence of the measurement. Given the relative ease of data acquisition in many measurements, data analysis often represents the greatest bottleneck in meaningfully relating the macroscopic polarization-dependent measurements back to molecular-scale structure. Some recent advances in this area are reviewed here, with a primary focus on intuitive but still fully quantitative molecular-level interpretations of NLO interactions.

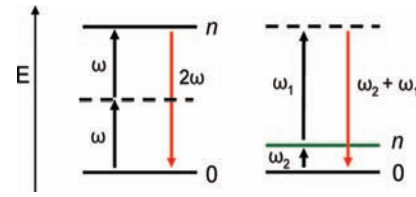

FIGURE 1. Energy level diagrams for SHG (left) and vibrational SFG (right).

The Molecular Response

Classical Anharmonic Oscillator Model. Before delving into the finer details of polarizability tensors derived from quantum mechanics, it makes sense to first start with a review of comparatively simple classical models of nonlinear optics. Frequency doubling is the conceptually simplest and practically most common NLO process and will be considered first. Classically, frequency doubling and mixing can be interpreted within the context of an anharmonic oscillator

* To whom correspondence should be addressed. E-mail: gsimpson@purdue.edu.
[†] Purdue University.
[‡] Indiana University–Purdue University Indianapolis.

Ronald D. Wampler received a B.S. in chemistry from the University of Virginia at Wise. He is currently pursuing his Ph.D. at Purdue University under the guidance of Prof. Garth J. Simpson. His research area focuses on chiral phenomenon in nonlinear optics.

Andrew J. Moad earned his B.S in Chemistry in 2001 from Indiana University and his Ph.D in Chemistry from Purdue University in 2006. Presently, he is a NRC postdoctoral fellow at the National Institute of Standards and Technology

Charles Moad holds a B.S. and M.S. in Computer Science from Indiana University. His focus is in computer graphics and distributed computing. He was an Associate Researcher for the Scientific Data Analysis Lab, a Pervasive Technology Lab of Indiana University. Currently he is an Applications Developer for the Indianapolis Museum of Art.

Randy Heiland received a M.S. in Computer Science from the University of Utah in 1985 and a M.A. in Mathematics from Arizona State University in 1992. He has developed software for scientific data visualization and analysis for nearly 25 years in industry, government labs, and academic research labs. Heiland is currently Associate Director of the Scientific Data Analysis (SDA) Lab, one of the Pervasive Technology Labs at Indiana University. Before joining IU in 2003, he was a senior research scientist in the Visualization and Virtual Environments group at NCSA/UIUC. Prior to NCSA, Heiland was a computer scientist in the Environmental Molecular Sciences Lab at the DOE Pacific Northwest National Lab. He has also held positions at the Los Alamos National Lab, Caterpillar Tractor Company, and an industrial research lab in Oslo, Norway.

Garth J. Simpson accepted an academic position in the Chemistry Department of Purdue University in 2001 and was promoted to Associate Professor in 2006. Notable recognitions include the Arthur F. Findeis Award from the American Chemical Society (2007), an Alfred P. Sloan Fellowship, a Cottrell Teacher–Scholar Award, a Beckman Young Investigator Award, a New Untenured Faculty Grantee Award from Eli Lilly, a Camille and Henry Dreyfus New Faculty Award, a Research Corporation Research Innovation Award, and the Victor K. LaMer Award by the American Chemical Society.

10.1021/ar600055t CCC: $37.00
Published on Web 08/23/2007

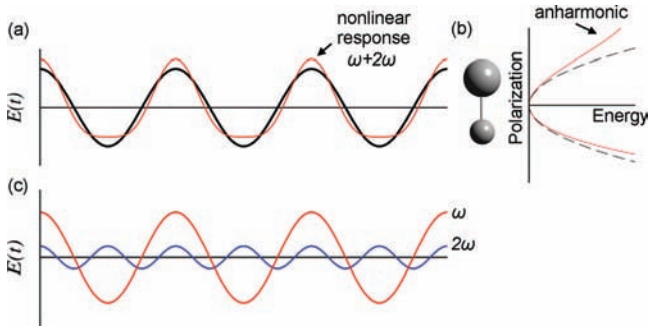

FIGURE 2. Classical anharmonic oscillator model describing second harmonic generation. Linear and nonlinear responses (a) and the anharmonic polarizability (b) for a hypothetical heteronuclear diatomic molecule. The nonlinear response shown in (a) in the time-domain is recovered by the summation of ω and 2ω (c).

such as the electron cloud polarizability of a heteronuclear diatomic molecule.[2] An illustration of this description is shown in Figure 2. For small driving amplitudes, the induced polarization of the electron cloud by the optical field is relatively small, and the harmonic terms in the polarizability dominate such that the molecular polarization tracks the driving frequency. However, for higher driving forces (e.g., stronger electric fields), the anharmonic terms become important. These terms arise from differences in the molecular polarizability on the upstroke of the field relative to the downstroke arising from asymmetry within the molecule. For example, if one atom of a heteronuclear diatomic molecule "holds" the electron cloud more tightly than the other, this difference in polarizability manifests itself as anharmonicity within the molecular polarizability, with the net resulting polarization shown as the red trace in Figure 2a.

The nonlinear polarizability depicted in Figure 2a is represented in the time domain. In the frequency domain, it should be obvious from inspection of Figure 2c that addition of a relatively small amount of a frequency-doubled contribution recovers the distortions expected by the anharmonicity, as long as the distortions are relatively small. Similar arguments also apply for classical descriptions of SFG when using two different driving frequencies.[2]

This hypothetical heteronuclear diatomic molecule represents the simplest possible SHG or SFG active system. In more complex molecules, the induced SHG polarization does not generally orient in the same direction as the driving field. The nonlinear polarization can be conveniently described by a vector in a Cartesian coordinate system, $\vec{P}_{NL}$. Since three Cartesian coordinates also describe each of the incident driving fields, a $3 \times 3 \times 3$ Cartesian tensor describes all possible nonlinear polarizations generated under all possible incident polarizations (i.e., a rank three tensor $\boldsymbol{\beta}_{ijk}$, each element of which describes the efficiency of generating a NLO polarization along the i-coordinate of the molecule when driven by incident fields polarized along the j and k molecular coordinates).

This simple classical model provides an intuitive framework for understanding many key aspects of frequency doubling and mixing at the molecular level. For example, the sign of the frequency-doubled light depends on the orientation of the oscillator. From inspection of Figure 2, two oppositely oriented anharmonic oscillators would generate SHG polarizations that exactly canceled. A sample comprised of many molecules with random orientations will result in complete cancellation of the SHG response. Furthermore, the classical model provides a foundation for interpreting SHG and SFG through rank 3 tensors.

Quantum Mechanical Models. Although intuitively appealing, the classical model for SHG and SFG does not clarify the underlying mechanism dictating the nonlinear polarizability of the electron cloud. It could be argued that the best place to start for developing an intuitive understanding of quantum mechanical models for the molecular NLO responses is with the computational algorithms used to generate them. In general, three different and complementary approaches have found wide-spread use: (1) adiabatic calculations performed in the limit of slowly varying or DC electric fields; (2) application of time-dependent perturbation theory to derive and calculate sum-over-states expressions for the molecular tensor; (3) contraction approaches that allow the resonant molecular tensor to be expressed as direct products of lower-order effects. These are certainly not the only methods of calculating the nonlinear polarizability, but they serve as illustrative examples describing the conceptual frameworks most often used to interpret the molecular origins of NLO phenomena.

Adiabatic Nonlinear Polarizability. In the first approach, the nonlinear polarizability tensor is calculated from partial derivatives of the molecular energy, H, with respect to the DC electric field, E.[3,4]

$$\beta_{ijk} = \frac{-\partial^3 H}{\partial E_i \partial E_j \partial E_k} \tag{1}$$

Equation 1 yields the adiabatic hyperpolarizability, in which the electron cloud responsible for the NLO polarization is assumed to respond fast relative to the time scale of the optical period. Another way of stating this limit is to say that the adiabatic approximation implicitly assumes that all electronic resonances are sufficiently high in energy that they yield equal contributions to the generation of both of the two virtual states.

The adiabatic calculations in the DC limit build on the success of loosely similar computational approaches for describing Raman tensors, in which the adiabatic Raman polarizability is calculated from the change in DC polarizability as bonds are translated along normal vibrational coordinates.[5,6] For most vibrational Raman transitions, this is a fairly good approximation, since the energy difference between virtual states for the Stokes and anti-Stokes Raman transitions equals just one vibrational quantum and the energies of the virtual states are typically much lower than electronic transitions. However, these same favorable conditions do not generally apply for electronic SHG and vibrational SFG. In SHG, the energies of the two virtual states (one at ω and one at 2ω) always differ by 100%, and the doubled frequencies often approach electronic resonances. As a result, the adiabatic hyperpolarizability is not particularly reliable for calcula-

tions of nonlinear polarizabilities. For example, one glaring inadequacy of the adiabatic hyperpolarizability calculated using eq 1 is its invariable prediction of fully symmetric molecular tensors with complete interchangeability of all the indices (i.e., Kleinman symmetric),[7] which is reasonably well established as being generally invalid under practical experimental conditions, even far from resonance.[8–10] Furthermore (and most importantly), the adiabatic polarizability does not allow for calculation of resonance-enhanced effects in SFG or SHG arising when either an incident or exigent frequency approaches resonance with a real transition within the molecule, which underlay virtually all NLO spectroscopy measurements.

Sum-over-States Expressions of Optical Nonlinearity. The most exciting aspects of molecular NLO phenomena often arise from resonance-enhanced spectroscopic measurements, for which the adiabatic expression in eq 1 clearly cannot apply. A very general treatment for describing resonant NLO interactions through the use of time-dependent response functions can be found in an excellent treatise by Mukamel (to cite just one source).[11] This general approach can be simplified considerably by assuming that each molecular excited state decays independently with a single-exponential time dependence (i.e., in the limit of a frozen matrix exhibiting inhomogeneous broadening such that the dynamic motion of the bath is either much faster or much slower than the excited state lifetimes of the individual molecules). It should be noted that this will not generally be a particularly good approximation in complex and highly coupled systems. However, the primary focus of the present work is on development of intuitive methods for interpreting polarization dependence in the frequency domain, which is not likely to be greatly affected by these interesting but comparatively subtle short-time inter- and intramolecular dynamic interactions. At the single-molecule level, exponential decays in the time domain translate to Lorentzian line shapes in the frequency domain, such that the molecular nonlinear polarizability can be written analytically as a double sum-over-states (SOS) with six terms for SFG (including SHG as a specific subset).[2,12,13]

$$\beta^{ijk}(-\omega_{\mathrm{sum}};\omega_a,\omega_b)=\frac{-1}{4\hbar^2}\sum_p\sum_q \left\{\frac{\mu^i_{0q}\mu^k_{qp}\mu^j_{p0}}{(\omega_q+\omega_{\mathrm{sum}}+i\Gamma_q)(\omega_p+\omega_a+i\Gamma_p)}+\frac{\mu^j_{0q}\mu^k_{qp}\mu^i_{p0}}{(\omega_q-\omega_a-i\Gamma_q)(\omega_p-\omega_{\mathrm{sum}}-i\Gamma_p)}+\frac{\mu^i_{0q}\mu^j_{qp}\mu^k_{p0}}{(\omega_q+\omega_{\mathrm{sum}}+i\Gamma_q)(\omega_p+\omega_b+i\Gamma_p)}+\frac{\mu^k_{0q}\mu^j_{qp}\mu^i_{p0}}{(\omega_q-\omega_b-i\Gamma_q)(\omega_p-\omega_{\mathrm{sum}}-i\Gamma_p)}+\frac{\mu^k_{0q}\mu^i_{qp}\mu^j_{p0}}{(\omega_q-\omega_b-i\Gamma_q)(\omega_p+\omega_a+i\Gamma_p)}+\frac{\mu^j_{0q}\mu^i_{qp}\mu^k_{p0}}{(\omega_q-\omega_a-i\Gamma_q)(\omega_p+\omega_b+i\Gamma_p)}\right\} \quad (2)$$

The nonlinear polarizability in eq 2 derived from time-dependent perturbation theory consists of two infinite summations over all excited states in the system and six triple products of transition moments, each of which contains a unique frequency-dependent response. Analogous expressions for higher-order NLO and multiphoton processes have significantly more terms, expressed as n-fold summations over $(n+1)!$ terms for an n-order NLO process (for example, a seven-wave mixing process is described by a sextuple summation over 5040 products of eight transition moments and corresponding frequency terms).

Despite the unwieldiness of the above equation and its analogs for higher-order effects, it contains a certain underlying physical elegance. The polarized molecule is not in an eigenstate. Therefore, the time dependence associated with the oscillatory polarization of this virtual state can be interpreted by a summation of eigenstates. Each eigenstate evolves at its own characteristic frequency ($\omega = E/\hbar$), the linear combination of which results in the time-dependent polarizability represented in Figure 2. Each triple product of transition moments in eq 2 corresponds one-to-one to a unique Feynman pathway connecting the initial state back to the initial state.[12,14] However, chemical intuition about the molecular interactions driving optical nonlinearity in molecular systems is not necessarily directly obvious from such explicit SOS expressions.

Contraction of Sum-over-States Equations. Underlying intuitive molecular mechanisms masked by full SOS expressions such as shown in eq 2 can often be unveiled by simple algebraic manipulations. By folding in one of the two infinite summations in eq 2, the same SOS expression can be recast identically in the following two equivalent contracted forms.[14,15]

$$\beta_{ijk}(-\omega_{\mathrm{sum}};\omega_a,\omega_b)=\frac{-1}{2\hbar^2}\sum_p\frac{(\alpha^{kj}_{0p})_{\mathrm{2PE}}\mu^i_{p0}}{\omega_{p0}+\omega_{\mathrm{sum}}+i\Gamma_p}+\frac{(\alpha^{ik}_{0p})_{\mathrm{AR}}\mu^j_{p0}}{\omega_{p0}-\omega_a-i\Gamma_p}+\frac{(\alpha^{\mathrm{ij}}_{0p})_{\mathrm{AR}}\mu^k_{p0}}{\omega_{p0}-\omega_b-i\Gamma_p}=\frac{-1}{2\hbar^2}\sum_q\frac{\mu^i_{0q}(\alpha^{jk}_{q0})_{\mathrm{2PA}}}{\omega_{q0}-\omega_{\mathrm{sum}}-i\Gamma_p}+\frac{\mu^j_{0q}(\alpha^{ki}_{q0})_{\mathrm{SR}}}{\omega_{q0}+\omega_a+i\Gamma_p}+\frac{\mu^k_{0q}(\alpha^{ji}_{q0})_{\mathrm{SR}}}{\omega_{q0}+\omega_b+i\Gamma_p} \quad (3)$$

In eq 3, the α terms refer to rank two tensors describing Stokes Raman (SR), anti-Stokes Raman (AS), two-photon absorption (2PA), or two-photon emission (2PE), indicated by the subscripts. The two expressions in eq 3 are each mathematically identical to eq 2, with no additional assumptions or approximations. In fact, it has recently been shown that SOS expressions for broad classes of NLO and multiphoton phenomena can be similarly contracted to comparatively simple sums of direct products of lower-order effects.[14,15]

Under conditions of single resonance enhancement with one of the incident frequencies (typical of vibrational SFG) or with the exigent frequency (typical of electronic SHG and SFG), the NLO analog of the rotating wave approximation (RWA) can be invoked to further simplify the expressions for the molecular tensor. In essence, all

the nonresonant interactions can be reasonably assumed to vary slowly with frequency across the line shape function of the resonance and can therefore be treated as a constant nonresonant background (i.e., the NLO equivalent of the refractive index). Invocation of the RWA results in the following expressions for vibrational SFG (resonant with ω_b) and electronic SHG (resonant with 2ω) for molecules initially in the ground state.[14–16]

$$\beta^{(2)}_{ijk}(-\omega_{\mathrm{sum}};\omega_a,\underline{\omega_b}) = \frac{-1}{2\hbar}\sum_n S_n(\omega_b)\cdot(\alpha^{ij}_{0n})_{\mathrm{AR}}\mu^k_{n0} \quad (4a)$$

$$\beta^{(2)}_{ijk}(-\underline{2\omega};\omega,\omega) = \frac{-1}{2\hbar}\sum_n S_n(2\omega)\cdot\mu^i_{0n}(\alpha^{jk}_{n0})_{\mathrm{2PA}} \quad (4b)$$

In eqs 4a and 4b, the line shape function S has been expressed generally, such that the equations are valid for line shapes other than Lorentzian (for Lorentzian line shapes, $S_n(\omega) = [\omega_n - \omega - i\Gamma_n]^{-1}$). The underscore inside the parenthetical indicates the resonance-enhanced condition for which the equations hold. The molecular tensors describing higher-order NLO or multiphoton effects may be similarly contracted to direct products of lower-order phenomena using identical methods.[14]

At this stage, we have basically just gone through an extensive exercise to rigorously derive the expressions in eqs 4a and 4b that we probably could have guessed just by direct inspection of the energy-level diagrams in Figure 1. In the case of vibrational SFG, the NLO process "looks" like it should consist of one-photon vibrational excitation coupled coherently to an anti-Stokes Raman transition, which is precisely the result obtained quantum mechanically by eq 4a. Similarly, in the case of electronic resonance enhancement, inspection of the energy-level diagram suggests that the molecular tensor is described by the coherent combination of two-photon absorption and stimulated emission, consistent with eq 4b. Although in retrospect it seems quite obvious, it is worth highlighting that a rigorous mathematical connection between two-photon absorption and SHG was only first demonstrated in 2004.[15] Most significantly for the present purposes, these different mathematical descriptions of the molecular hyperpolarizability (adiabatic, sum-over-states, and contracted expressions) allow for the use of visual representations using different and complementary approaches, described in the next sections.

Visualization of Linear and NLO Tensors

Several established tools originally developed for visualizing Raman (and related) tensors provide a convenient framework for extension to higher-order NLO phenomena.[5] Therefore, it makes sense to provide a brief review of common methods for visually representing the polarization dependence of Raman spectroscopy. Under the most common conditions in the adiabatic limit, the Raman tensor can be reasonably described by a symmetric (or more generally, Hermitian) 3×3 matrix.[5] This matrix can be represented visually by a polarizability ellipsoid, the principal axes of which parallel the eigenvectors of the symmetric matrix (Figure 3).[5] In the present formulation, the distance from the origin along any direction in the ellipsoid effectively describes the efficiency of generating a Raman electric field polarization in that direction when driven by a coparallel incident field (please note that this definition differs somewhat from common definitions for Raman polarizability ellipsoids[5]). Alternatively, the same information can be concisely conveyed through the use of three double-sided arrows representing the three principal moments of the Raman tensor. The directions parallel the eigenvectors and the lengths indicate the magnitude of the corresponding eigenvalues, shown in Figure 3. The ellipsoid representations and the diagrammatic approaches contain equivalent information, both of which completely and quantitatively describe the polarization dependence of Raman in the limit of a symmetric tensor.

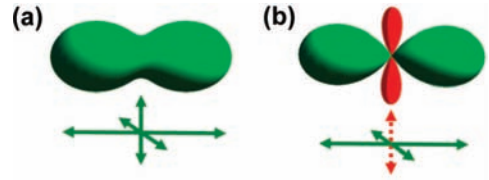

FIGURE 3. Ellipsoid and diagrammatic representation of $\alpha^{(1)}$ tensors, such as those describing Raman (a) and TPA (b).

Because Raman and two-photon absorption (TPA) are both described by rank 2 tensors; these same visualization tools are equally applicable for representing the polarization dependence of TPA. Whereas the eigenvalues of the Raman tensor are often like-signed, resulting in "squashed football" polarizability ellipsoids (Figure 3a), TPA tensors often exhibit sign changes between principal elements, such that the polarizability ellipsoids routinely exhibit "clover-leaf" structures (Figure 3b). Interestingly, these sign changes result in nodes. In the case of TPA, this node corresponds to an angle for which linearly polarized light is predicted to exhibit a minimum in the two-photon excitation cross-section.

Extension of Visualization Techniques to Second-Order NLO Phenomena. With this review of previous methods for visualizing rank 2 Raman and TPA tensors in place, attention can now be turned to interpreting rank 3 SHG and SFG tensors using a similar toolkit. At the molecular level, the resonant nonlinear polarizability tensor is given through eq 4a as the line shape function multiplied by the direct product of the transition moment and either the TPA or Raman tensor (depending on whether the resonant interaction is with ω_{sum} or ω_b, respectively). Consequently, quantitative representations of resonant $\boldsymbol{\beta}^{(2)}$ tensors can be generated simply by including the vector indicating the transition moment in combination with the diagrammatic representations of the Raman or TPA tensors described previously.[17,18] This arrow representation is much more than just a visual aid for qualitatively interpreting polarization-dependent NLO effects; it is a complete and rigorous quantitative representation of the resonant $\boldsymbol{\beta}^{(2)}$ tensor. Projection of these arrows onto any particular selection of Cartesian coordinates in combination with the line shape function allows quantitative reconstruction of all 27 unique nonzero

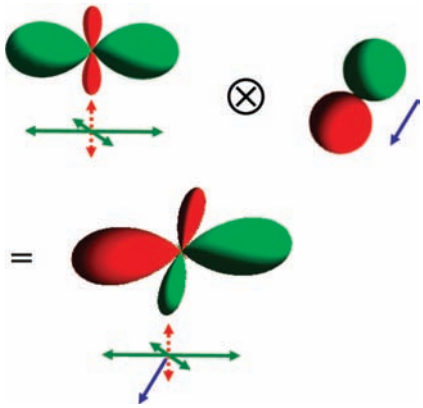

FIGURE 4. Hyperellipsoid (bottom) arising from the direct product of the TPA tensor (left) and the transition moment (right).

resonance-enhanced tensor elements present in that coordinate system as a function of wavelength.[17]

The polarizability ellipsoids used to visually represent Raman (and TPA) tensors through space-filling structures also have direct analogs in higher-order optical effects, exemplified in Figure 4. In this case, the distance from the origin of the hyperellipsoid indicates the magnitude of the sum or second harmonic frequency field in any direction when generated with coparallel incident fields, with green indicating positive sign and red negative sign. As in the Raman and TPA cases, these hyperellipsoid representations are fully quantitative, containing much of the same information as the diagrammatic representations using arrows (some of the chiral contributions are not recovered by the hyperellipsoids of $\boldsymbol{\beta}^{(2)}$ tensors).

The shapes of the hyperellipsoids can be conveniently interpreted by considering the transition moments and the TPA and Raman tensors. From inspection of Figure 4, the direct product of the transition moment (represented by the analog of a p-type atomic orbital) with the TPA or Raman ellipsoid recovers the shapes of the hyperellipsoids. For example, multiplication of the main positive lobes in the $\boldsymbol{\alpha}^{(1)}$ tensor by the transition moment results in a positive product on the right and a negative product on the left in the $\boldsymbol{\beta}^{(2)}$ tensor. The negative minor lobes in the $\boldsymbol{\alpha}^{(1)}$ tensor undergo similar transformations upon multiplication by $\boldsymbol{\mu}$, with the double negative in the downward direction resulting in a positive lobe, etc.

Optical Nonlinearity in Systems of Multiple Chromophores

Up to this point, discussion has focused on building up the tools for representing the NLO properties of single chromophores. Now, efforts are turned to considerations of visualizing the polarization-dependent NLO responses of systems of many coupled chromophores, starting with dimers, followed by semi-infinite polymers, and finally surface and bulk assemblies. In this section, a perturbation theory approach is described for treating the NLO properties of all of these assemblies (from dimers to macroscopic surfaces and materials) using one simple toolbox.

Dimer Consisting of Two Coupled Chromophores. Coupling between two identical monomers to form a dimer serves as an excellent intuitive starting point when working toward extended polymeric systems. It makes sense to first review the role of coupling on the linear optical properties in a dimer before tackling the NLO properties. In brief, coupling between two chromophores in a dimer generates sum and difference exciton states, described by the positive and negative addition of the different initially degenerate ground- and excited-state wave functions of the monomers. Depending on the strength of coupling, these interactions can have a negligible or a profound impact on the polarization dependence of the NLO tensor. The weak coupling limit is easiest to handle, so it will be considered first. In the following discussion, "weak coupling" is defined pragmatically based on the energy splitting ($\Delta\hbar\omega$) arising from coupling between chromophores compared with the experimental line width of the resonance. In the limit of a frequency shift from exciton coupling, $\Delta\omega$, that is much less than the resonant line width, Γ (i.e., $\Delta\omega \ll \Gamma$), the two exciton peaks cannot be independently resolved spectroscopically, and the total NLO response will be approximately equal to that expected from multiple uncoupled frequency-degenerate chromophores. In this weak-coupling limit, the macromolecular NLO activity is simply given by coherent summation of all the individual monomer contributions, often expressed by orientational averages.[2,18] If the coupling is sufficiently strong (i.e., $\Delta\omega \geq \Gamma$), the NLO properties of the individual spectroscopically resolved exciton states can still be reliably recovered by simple orientational averaging combined with phenomenological treatment of the influence of coupling.[17,19] In this case, the polarization dependence can still be interpreted to first order by simply adding up all the contributions in the absence of coupling, then allowing the resulting sum and difference states to separate in energy.

The transition moments of two isolated exciton states in a dimer will generally be orthogonally polarized, given by the vector sum and difference of the two identical monomer transition moments (Figure 5). Similarly, the TPA or Raman tensors of the individual exciton states are also described by sums and differences of the monomer tensors, with the addition and subtraction made a bit more interesting by the use of matrices. Nevertheless, inspection of the resulting $\boldsymbol{\alpha}^{(1)}$ tensors for the sum and difference exciton states in Figure 5 yields diagrammatic representations and ellipsoids consistent with what one might have guessed for the sums and differences of the monomer tensors. Once $\boldsymbol{\mu}^{(0)}$ and $\boldsymbol{\alpha}^{(1)}$ have been determined for each exciton state, the second-order nonlinear polarizability is simply given by direct product of $\boldsymbol{\mu}^{(0)}$ and $\boldsymbol{\alpha}^{(1)}$ according to eq 4a and 4b. Previous computational and experimental studies of the coupling in binaphthol and in amide models for proteins support the quantitative reliability of this perturbation theoretical approach in second-order nonlinear optics.[17,19,20]

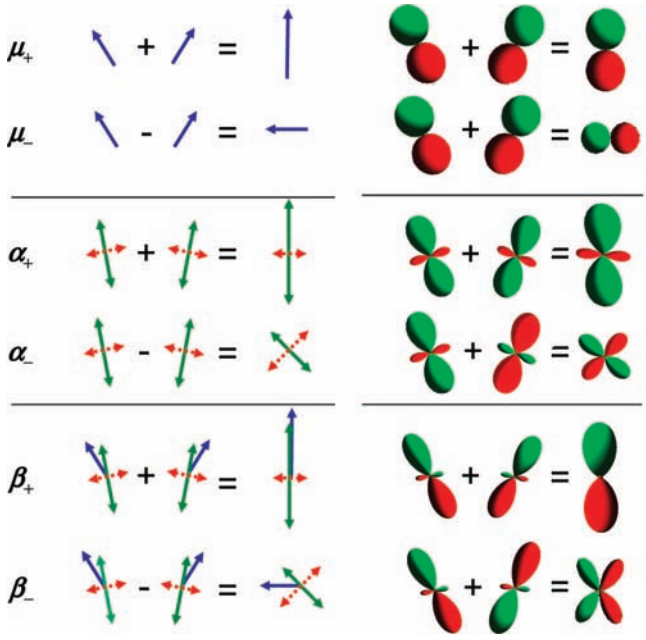

FIGURE 5. Diagrammatic representations for predicting the polarization-dependent electric dipole allowed absorption (described by $\boldsymbol{\mu}_+$ and $\boldsymbol{\mu}_-$), Raman and TPA (described by α_+ and α_-), and SFG and SHG (described by $\boldsymbol{\beta}_+$ and $\boldsymbol{\beta}_-$) of different exciton states in a dimer. The diagrammatic representations are shown to the left, and the corresponding surface representations to the right (see text for details). The antisymmetric contributions (not shown) can be similarly treated by simple vector addition as described in Figure 3.

The preceding discussion focused on reconstruction of the exciton $\boldsymbol{\beta}^{(2)}$ tensors by independent evaluation of $\boldsymbol{\mu}^{(0)}$ and $\alpha^{(1)}$ tensors for the different exciton states. However, the order of operations can be reversed with the same net result. In other words, this same methodology can also be performed from addition or subtraction of the monomer $\boldsymbol{\beta}^{(2)}$ tensors directly (Figure 5). However, use of the monomer $\boldsymbol{\beta}^{(2)}$ tensors extends the applicability of this perturbation theory approach to adiabatic (or other) calculations of the monomer hyperpolarizability.

Figure 5 serves to highlight some distinct advantages of these visual methods for describing coupled systems. Both the arrow and hyperellipsoid visual representations allow the tensors describing the individual exciton transitions to be represented *quantitatively* by projections of the individual monomer responses. More significantly, these visual methods, combined with the validity of perturbation theory, facilitate the interpretation of the polarization dependence of coupled systems simply by direct inspection of the monomer tensors and their relative orientation.

An explicit example for this procedure is shown in Figure 6, in which the NLO response of the exciton states in *N*-acetyl-*N*′-methyl glycyl amide (di-NMA) are compared with the tensors predicted from perturbation theory by summation of the individual monomer *N*-methylacetamide (NMA) tensors.[17] The tensors describing the independent $\pi \rightarrow \pi^*$ electronic transitions in the NMA monomers are shown in Figure 6. This transition generates two exciton states in the dimer, corresponding to the pairwise addition and subtraction of the excited eigenstate

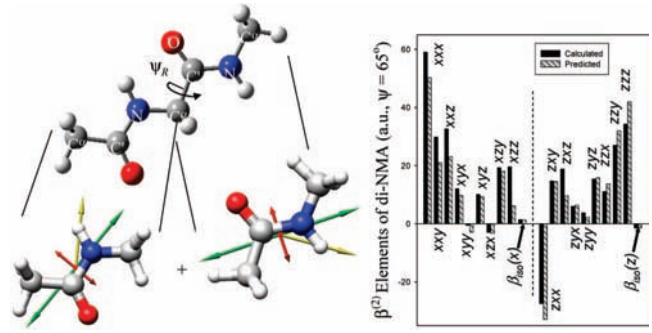

FIGURE 6. Comparison of the resonant tensors for the NV_1 $\pi \rightarrow \pi^*$ transitions in the di-NMA predicted by perturbation theory from the monomer response (Predicted) and those obtained by direct quantum chemical calculations of the fully coupled system (Calculated).

wave functions. The diagrammatic representation of the symmetric additive contribution in di-NMA is generated by directly summing the appropriately oriented monomers as depicted in Figure 6. Similarly, the NLO tensor for the other exciton transition is given by the difference. The tensors derived from perturbation theory in this manner matched up remarkably well with those obtained directly from quantum chemical calculations of the fully coupled dimer, also shown in Figure 6.

Extended Polymeric Systems. Once the effort of developing a formalism for treating coupling in dimers has been expended, it is remarkably straightforward to extend these approaches to semi-infinite repeating assemblies containing many identical coupled chromophores. Biopolymers and proteins serve as interesting representative models for algorithms that can be applied to diverse arrays of polymeric systems. An α-helix is formally a 3.6_{13} helix, with a repeat unit consisting of 18 monomers. Within the electric dipole approximation for light, the translation of a few angstroms of each chromophore along the helix chain is inconsequential, such that the NLO properties are dominated by the relative orientation of each monomer within the polymer. The improper C_{18} rotation axis yields the same symmetry as a C_∞ axis in second-order nonlinear optics, such that three exciton states are expected to emerge; one with the transition moment polarized along the helix axis and a doubly degenerate pair polarized perpendicular to the helix axis.

Exciton splitting can potentially play a significant role in describing the NLO properties of the electronic excited states, in which the exciton coupling is relatively strong. If the individual exciton states can be spectroscopically resolved, the polarizationdependence of each state is given by projection and summation of the monomer contributions through orientational averages.

A depiction of this process for an α-helix and the corresponding calculations for the $\boldsymbol{\beta}^{(2)}$ tensor of the polymer are given in Figure 7. With the validity of perturbation theory for treating coupling between amide subgroups having been confirmed (e.g., through calculations such as those shown in Figure 6), the nonlinear optical properties of extended biopolymers can be calculated using the same approach as for the dimer, but with significantly more monomeric units.

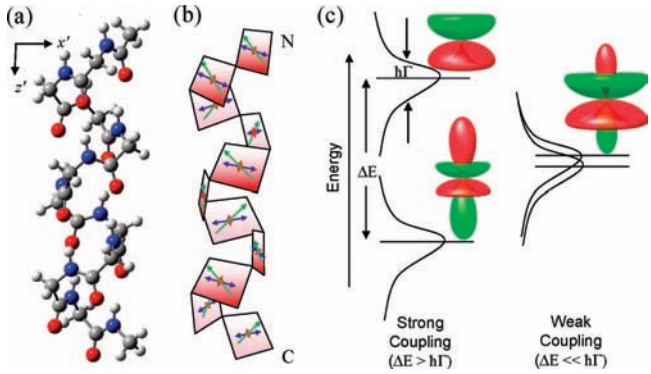

FIGURE 7. Ball and stick (a) and the diagrammatic (b) representations (shown here for the electronic NV1 π–π^* transition) of the α-helix. Hyperellipsoids for the strong and weak coupled exciton states of an α-helix (c).

In the case of the α-helix in Figure 7, the shapes of the hyperellipsoids shown in Figure 7c can be understood by inspection of the diagrammatic representations in Figure 7b. Considering first the contributions from the transition moments, vector addition of the single-sided green arrows shown in the figure will result in a transition moment pointing toward the top of the page aligned along the helix axis. Similarly, subtraction of any pair of transition moments on opposite sides of the helix results in a transition moment oriented orthogonal to the helix axis. Coherent addition of the TPA ellipsoids will generate a TPA ellipsoid for the sum state with a symmetric negative lobe aligned along the helix axis and an orthogonal positive lobe running symmetrically about the helix (qualitatively similar to a d_{z^2} atomic orbital). The direct product of these two will result in the hyperellipsoid shape depicted to the right for the lower-energy sum state. Similar arguments can be made for describing the difference state but are a bit more complicated to concisely describe because of the phase shift in the transition moment that arises as a function of rotation about the helix axis.

In the limit of weak splitting, the situation is even easier. The net NLO tensor given by the sum of the two exciton states corresponds exactly with what one would obtain simply by taking the orientational average of the monomers (i.e., in the absence of any significant coupling), also depicted in the figure on the far right. In vibrational SFG, these exciton states typically fall in the weak-coupling limit, such that the individual vibrational states cannot be independently resolved spectroscopically. In this limit, the NLO properties are simply given by coherent addition of the different monomer contributions within the protein through orientational averaging, and the role of exciton coupling can be neglected.

Macroscopic NLO Surface Response. Although the development of molecular-level descriptions of chiral effects in SHG and SFG is a critical first step, NLO measurements are invariably made on assemblies of many chromophores rather than on single molecules. The connection between the laboratory-frame NLO susceptibility of a thin film or material and the molecular-frame nonlinear polarizability can be approximated by the coherent addition of the contributions from the individual molecular responses.[2,18]

$$\chi_{IJK} = N_s \sum_{ijk} \langle R_{Ii} R_{Jj} R_{Kk} \rangle \beta_{ijk} \tag{5}$$

The coordinate transformation matrices represented by **R** in eq 5 connect the molecular and macroscopic frames by the three Euler angles θ, ψ, and ϕ, describing the tilt, twist, and azimuthal rotation angles, respectively. Equation 5 simply describes the macroscopic NLO response of a surface assembly or material in the weak coupling limit and is generally applicable provided that the energy splitting from intermolecular interactions is much less than the full width at half-maximum (FWHM) of the corresponding spectral line shape. Consequently, many of the same visualization tools developed for interpreting polymer responses can also be used directly for the interpretation of the macroscopic NLO properties of the surface assemblies. In this case, the hyperellipsoids describe the macroscopic polarization-dependent NLO activities of whole assemblies.

Complications from Linear Optical Properties

In practice, the conceptually simple descriptions presented in the preceding sections mask many practical complications associated with experimentally determining the $\chi^{(2)}$ tensor in eq 5. First, SHG and SFG measurements do not directly yield the $3 \times 3 \times 3$ Cartesian tensor in eq 5, but rather probe a $2 \times 2 \times 2$ Jones tensor that relates the Jones vector of the detected nonlinear polarization to the Jones vectors of the two driving fields (which are degenerate in SHG). By direct analogy with the linear optical properties of thin films in the absence of scattering, the Jones tensor describes the complete set of observables present in a single nonlinear optical measurement.[21,22] In the limit of a very thin film (much less than the wavelength of light), transformation from a Jones tensor to a Cartesian tensor given by eq 5 generally require precise knowledge of the optical constants of the ultrathin film.[18,23,24] For films only a single molecular layer in thickness, independent determination of these optical constants can be nontrivial. For thicker films and macroscopic materials, the linear optical constants can be obtained more precisely, but the simplifying assumptions afforded by sheet models no longer hold, and new complications associated with birefringence, interference, and phase-matching conditions emerge.

Perspectives and Outlook

Polarization analysis in nonlinear optics will continue to become an increasingly important element of this still-emerging discipline, the potential of which remains largely untapped. It is our hope that this review will help to foster this growth process by facilitating more intuitive molecular-level descriptions of polarization-dependent NLO and multiphoton processes that still retain the mathematical rigor of analytical expressions. Clearly, NLO measurements access information that is unique from and complementary to traditional linear spectroscopic and polarization-dependent methods. Polarization analysis in linear optics

of thin films has led to a powerful characterization technique in linear ellipsometry. Interference effects within thin films underpin the development of antireflection coatings, dichroic mirrors, and compact discs (among countless other advances). Polarization-dependent measurements in Raman spectroscopy provide elegant information on molecular symmetry and structure. By comparison, comparable approaches for describing and utilizing polarization-dependent interactions in nonlinear optics are still in their infancy. Polarization characterization and measurement in nonlinear optics will continue to be areas of active development for several years to come, motivated by the unique information content and fueled by increasing advances in capabilities of fast and ultrafast laser sources.

The authors gratefully acknowledge financial support from the National Science Foundation (CHE), the Research Corporation (Cottrell Teacher-Scholar Award), the Beckman Foundation (Young Investigator Award), and Eli Lilly (Analytical Chemistry Academic Contact Committee New Untenured Faculty Award) and a Lilly Endowment (IPCRES Initiative).

References

(1) Franken, P. A.; Hill, A. E.; Peters, C. W.; Weinreich, G. Generation of Optical Harmonics. *Phys. Rev. Lett.* **1961**, *7*, 118–119.
(2) Shen, Y. R. *The Principles of Nonlinear Optics*; John Wiley & Sons: New York, 1984.
(3) Rice, J. E.; Amos, R. D.; Colwell, S. M.; Handy, N. C.; Sanz, J. Frequency Dependent Hyperpolarizabilities with Application to Formaldehyde and Methyl Fluoride. *J. Chem. Phys.* **1990**, *93*, 8828–8839.
(4) Rice, J. E.; Handy, N. C. The Calculation of Frequency-Dependent Polarizabilities as Pseudo-Energy Derivatives. *J. Chem. Phys.* **1991**, *94*, 4959–4971.
(5) Long, D. A. *The Raman Effect. A Unified Treatment of the Theory of Raman Scattering by Molecules*; John Wiley and Sons: New York, 2002.
(6) Born, M.; Oppenheimer, R. Zur Quantentheorie Der Molekeln. *Ann. Phys.* **1927**, *84*, 457–484.
(7) Kleinman, D. A. Nonlinear Dielectric Polarization in Optical Media. *Phys. Rev.* **1962**, *126*, 1977–1979.
(8) Dailey, C. A.; Burke, B. J.; Simpson, G. J. The General Failure of Kleinman Symmetry in Practical Nonlinear Optical Applications. *Chem. Phys. Lett.* **2004**, *390*, 8–13.
(9) Zhang, W.-K.; Zheng, D.-S.; Xu, Y.-Y.; Bian, H.-T.; Guo, Y. W. H.-F. Reconsideration of Second Harmonic Generation from Isotropic Liquid Interface: Broken Kleinman Symmetry of Neat Air/Water Interface from Dipolar Contribution. *J. Chem. Phys.* **2005**, *123*, 224713.
(10) Franken, P. A.; Ward, J. F. Optical Harmonics and Nonlinear Phenomena. *Rev. Mod. Phys.* **1963**, *35*, 23–39.
(11) Mukamel, S. *Principles of Nonlinear Optical Spectroscopy*; Oxford University Press: New York, 1995.
(12) Ward, J. F. Calculation of Nonlinear Optical Susceptibilities Using Diagrammatic Perturbation Theory. *Rev. Mod. Phys.* **1965**, *37*, 1–18.
(13) Butcher, P. N.; Cotter, D. *The Elements of Nonlinear Optics*; Cambridge University Press: New York, 1990.
(14) Moad, A. J.; Simpson, G. J. Self-Consistent Approach for Simplifying the Interpretation of Nonlinear Optical and Multiphoton Phenomena. *J. Phys. Chem. A* **2005**, *109*, 1316–1323.
(15) Moad, A. J.; Simpson, G. J. A Unified Treatment of Symmetry Relations and Selection Rules in Sum-Frequency and Second Harmonic Spectroscopies. *J. Phys. Chem. B* **2004**, *108*, 3548–3562.
(16) Hirose, C.; Akamatsu, N.; Domen, K. Formulas for the Analysis of Surface Sum-Frequency Generation Spectrum by Ch Stretching Modes of Methyl and Methylene Groups. *J. Chem. Phys.* **1992**, *96*, 997–1004.
(17) Perry, J. M.; Moad, A. J.; Begue, N. J.; Wampler, R. D.; Simpson, G. J. Electronic and Vibrational Second-Order Nonlinear Optical Properties of Protein Secondary Structural Motifs. *J. Phys. Chem. B* **2005**, *109*, 20009–20026.
(18) Moad, A. J.; Moad, C. W.; Perry, J. M.; Wampler, R. D.; Begue, N. J.; Shen, T.; Goeken, G. S.; Heiland, R.; Simpson, G. J. NLOPredict: Visualization and Data Analysis Software for Nonlinear Optics. *J. Computational Chem.* **2007**, *28*, 1996–2002.
(19) Heinz, T. F. *Nonlinear Surface Electromagnetic Phenomena*; North-Holland: New York, 1991; pp 354–416.
(20) Simpson, G. J.; Perry, J. M.; Moad, A. J.; Wampler, R. D. Uncoupled Oscillator Model for Interpreting Second Harmonic Generation Measurements of Oriented Chiral Systems. *Chem. Phys. Lett.* **2004**, *399*, 26–32.
(21) Belkin, M. A.; Shen, Y. R.; Flytzanis, C. Coupled-Oscillator Model for Nonlinear Optical Activity. *Chem. Phys. Lett.* **2002**, *363*, 479–485.
(22) Plocinik, R. M.; Everly, R. M.; Moad, A. J.; Simpson, G. J. A Modular Ellipsometric Approach for Mining Structural Information from Nonlinear Optical Polarization Analysis. *Phys. Rev. B* **2005**, *72*, 125409.
(23) Dehen, C. J.; Everly, R. M.; Plocinik, R.; Simpson, G. J. Discrete Retardance Second Harmonic Ellipsometry. *Rev. Sci. Instrum.* **2007**, *78*, 013106.
(24) Polizzi, M. A.; Plocinik, R. M.; Simpson, G. J. Ellipsometric Approach for the Real-Time Detection of Label-Free Protein Adsorption by Second Harmonic Generation. *J. Am. Chem. Soc.* **2004**, *126*, 5001–5007.
(25) Polizzi, M. A.; Plocinik, R. M.; Simpson, G. J. Correction: Ellipsometric Approach for the Real-Time Detection of Label-Free Protein Adsorption by Second Harmonic Generation. *J. Am. Chem. Soc.* **2005**, *127*, 1058.

AR600055T